Title

Implications of mHVSR Spatial Variability on Site Response Predictability

Authors

Ornelas, Francisco Javier
de la Torre, Christopher A
Stewart, Jonathan P

Publication Date

2024-10-17

Peer reviewed

IMPLICATIONS OF mHVSR SPATIAL VARIABILITY ON SITE RESPONSE PREDICTABILITY

Francisco Javier G. Ornelas[1], Christopher A. de la Torre[2], Jonathan P. Stewart[1]

[1] *Department of Civil & Environmental Engineering*
University of California, Los Angeles, USA
[2] *Department of Civil & Natural Resources Engineering*
University of Canterbury, Christchurch, NZ

Abstract

One-dimensional ground response analyses (GRA) can introduce model error to site response estimates when wave propagation is not dominated by vertically propagating shear waves. We identify sites suitable for GRA based on microtremor horizontal-to-vertical spectral ratios (mHVSRs). We analyzed 300 microtremor recordings from 17 vertical array sites in California, comparing mHVSRs at varying spatial separations. We find that low mHVSR spatial correlation, as measured using Longest Common Subsequence, tends to occur at vertical array sites that are poorly modeled by GRA. Conversely, stronger mHVSR correlations tend to occur at sites where GRA is relatively effective.

Keywords: horizontal-to-vertical spectral ratios, ground response analysis, site response, spatial variability

Introduction

One-dimensional (1D) ground response analyses (GRA) are commonly applied for evaluating the effects of site response on ground shaking. These 1D analyses rely on the assumptions that the soil profile is made up of laterally continuous horizontal layers and the wavefield is comprised of only vertically-propagating shear waves. Previous studies have evaluated the effectiveness of 1D GRA at vertical array sites in Japan (Thompson et al. 2012; Kaklamanos et al. 2013; Pilz and Cotton, 2019; Tao and Rathje 2020a) and California (Teague et al. 2018; Afshari and Stewart 2019; Tao and Rathje 2020a; Stewart and Afshari 2021; de la Torre et al. 2022). Many of these studies have found that the site response predicted by 1D GRA does not accurately capture observed transfer functions from appreciable fractions of the vertical array sites and overpredicts transfer function ordinates near fundamental mode frequencies.

Misfits of 1D GRA to observation can be attributed to complexities of the soil profile and wave field that are difficult to anticipate in advance for sites without vertical arrays (i.e., most sites for which seismic hazard analyses are to be performed). To address this, a number of recent SSHAC projects have incorporated model error into their logic trees. This model error represents epistemic uncertainty in the use of 1D GRA as the basis for site response modeling. Using data from California sites, a model for model error was developed by Stewart and Afshari (2021), which has subsequently been confirmed by Bahrampouri and Rodriguez-Marek (2023) using data from Kik-net sites in Japan when reasonable levels of V_S profile variability are considered in the data

interpretation. The approximate level of model error at periods shorter than the soil column period is 0.3 natural log units, which is appreciable. Such high levels of model error represent network averages, whereas some individual sites are known to be relatively accurately modelled by 1D GRA. For such sites, lower levels of model error in principle could be technically defensible. However, for this to be realized would require site characterization methods that can be used to evaluate whether a site will behave in a relatively one-dimensional manner. In the absence of abnormally extensive site characterization (i.e., many closely spaced invasive tests to measure V_S profiles), we currently lack such methods.

In this study, we investigate the use of microtremor Horizontal-to-Vertical Spectral Ratios (mHVSR) at a series of locations across a site as a means by which to assess site heterogeneity. For each of 17 vertical array sites in California, mHVSR was measured near the array and at a series of stations at distances of approximately 50, 100, 250 and 500 m from the array in an approximately circular pattern (12-16 locations per site in total). We propose repeatable metrics by which to interpret spatial variations of mHVSR across these locations and apply them to a dataset of 300 microtremor measurements from the 17 vertical sites. Using data from prior studies, we re-evaluate the goodness-of-fit of empirical and theoretical transfer functions from the vertical arrays to identify sites with and without good match of 1D GRA to the data. Finally, we perform preliminary tests of the hypothesis that mHVSR spatial variability metrics correlate to 1D GRA modeling effectiveness.

Methodology for Spatial Measurement and Interpretation of mHVSR

HVSR is an economical technique for seismic site characterization, employing a three-component seismic instrument that records ambient ground vibrations over a relatively brief duration (~ 1-2 hours) in two horizontal directions and vertically. Fourier amplitude spectra (FAS), and the ratio of horizontal-to-vertical FAS are computed. Originally proposed by Nogoshi and Igarashi (1971) and later popularized by Nakamura (1989), HVSR reveals site resonances if horizontal components of seismic waves are amplified by sites to a greater degree than vertical components. HVSR that is based on ambient vibrations from microtremors or anthropogenic sources is commonly termed mHVSR to differentiate it from HVSR derived from earthquakes (eHVSR).

Numerous studies have found that the lowest frequency peak observed in mHVSR often correlates with the fundamental shear wave resonant frequency (f_0) of the site (Lermo and Chavez-Garcia 1993; Lachet and Bard 1994; Ghofrani et al. 2013; Molnar et al. 2018). Ordinates from mHVSR have also been used in empirical models as predictors of site response (e.g., Pinilla-Ramos et al. 2022; Wang et al. 2022a; Buckreis et al. 2024). Here a different application of mHVSR is discussed, as a low-cost indicator of site heterogeneity.

Sites considered and mHVSR data collection

We utilize a California vertical array database (Afshari et al. 2019) that consists of 21 sites, which are primarily located near major highway bridges. These sites have time-averaged shear-wave velocities in the upper 30 m (V_{S30}) ranging from 160-810 m/s, with 10 sites being less than 300 m/s (Afshari and Stewart 2019).

From 17 of these sites, 300 microtremor measurements were performed, 16 from (Ornelas et al. 2023) and 1 from Prof. Brady Cox (personal communication, 2024). These measurements are archived in the shear wave velocity profile database (VSPDB) (Kwak et al. 2021). Figure 1 shows the locations of each of these stations and Table 1 provides details of each site, including the mHVSR measurement identification number in the relational database (e.g., VSPDB ID).

Table 1. Attributes of vertical array sites in California used in this study

Station No.	CSMIP Station No.	VSPDB ID	Station Name	V_{S30} (m/s)	Latitude	Longitude
2	68323	1783	Benicia-Martinez South	547	38.03351	-122.117
3	68206	1801	Crockett-Martinez	335	38.05394	-122.225
4	1794	1818	El Centro-Meloland	238	32.77393	-115.449
7	UCSB Arrays	1835	Hollister	385	36.75758	-121.613
8	58798	1865	Hayward-San Mateo	185	37.61694	-122.154
9	24703	1869	La Cienega	242	34.03621	-118.378
10	24400	1874	Obregon Park	452	34.03701	-118.178
11	23792	1875	San Bernardino	252	34.06369	-117.298
12	68310	1891	Vallejo-Hwy 37	528	38.1217	-122.275
13	UCSB Arrays	NA	Wildlife Liquefaction Array	200	33.097	-115.53
14	67266	1909	Antioch-San Joaquin S.	253	38.01792	-121.751
15	13186	1923	Corona	321	33.88171	-117.549
16	3192	1939	Coronado East	329	32.69825	-117.145
17	3193	1954	Coronado West	214	32.68815	-117.164
18	58798	1968	Foster City-San Mateo	810	37.57276	-122.264
19	58487	1986	Hayward-580W	489	37.68868	-122.107
20	58961	2006	San Francisco Bay Bridge	391	37.7866	-122.389

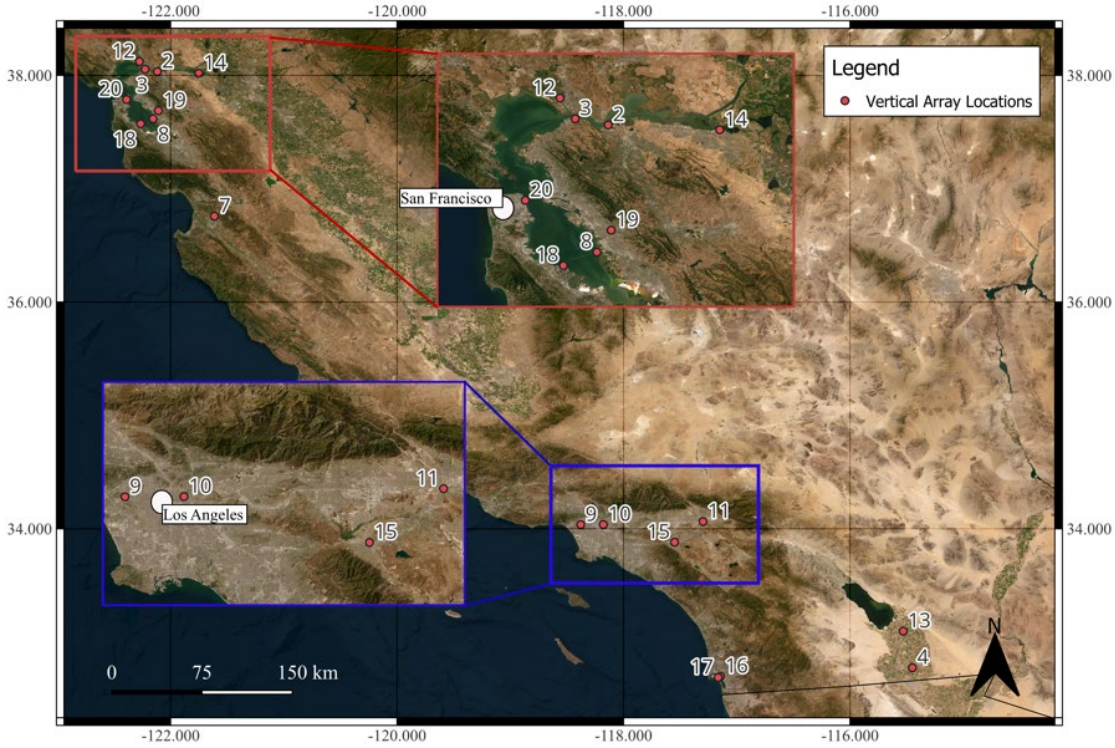

Figure 1. Locations of vertical array sites used in this study

Instruments in these mHVSR arrays were configured in a concentric circle layout, with the center instrument near the vertical array and others at radii of 50, 100, 250, and 500 m. We attempted to collect data from at least four locations around each circle for about 1-2 hours each at different times. However, in some cases, we were constrained by bodies of water and restricted access to properties (typically private property). The naming convention of the tests used was based on the site, the distance from the array, and the index of the test. For example, testing at site 2 and radius 50 m was named 2.50.1. A test at the vertical array or close to it would be 2.0.0, meaning that it is 0 m away and the only test taken there. Figure 2 shows the test layouts for sites in the Martinez Bay Area (Figure 2a) and El Centro-Meloland in Imperial Valley (Figure 2b). Figure 2a shows an example of the limitations that occurred while collecting the microtremor data, where some of the desired locations are in a nearby waterbody or private property.

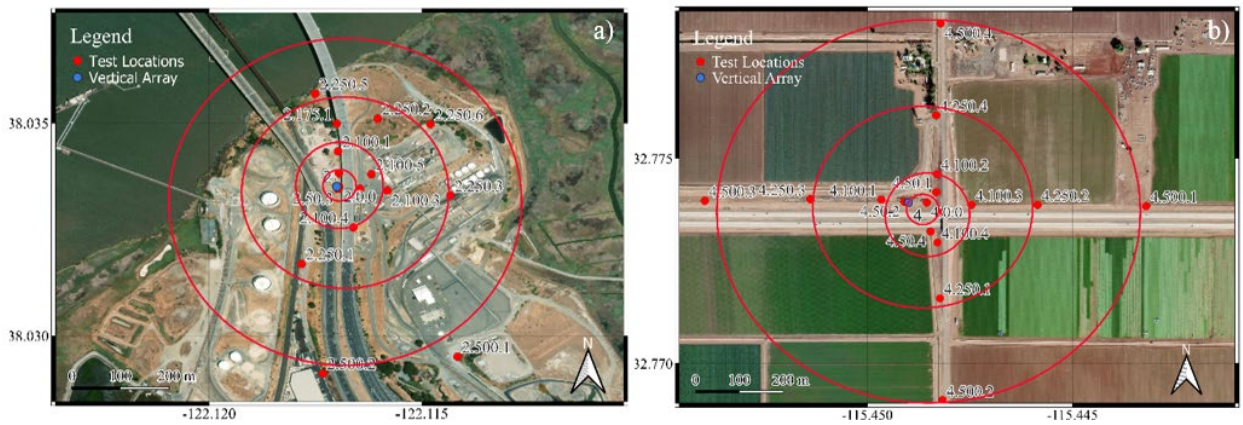

Figure 2. Layout of mHVSR measurement locations: (a) plan view of site in Benicia-Martinez (site 2), showing the limitations in the collection of data; (b) plan of site in El Centro-Meloland (site 4), showing a layout where all tests were performed at the site. Numbers indicate test names -- the first digit indicates the station number, the second indicates the distance from the vertical array, and the last indicates the index of the test.

The temporary surveys were performed with deployments of Nanometrics Trillium Compact Horizon 120s 3-component broadband seismometers with Pegasus PGS-140 dataloggers. These seismometers have a flat frequency bandwidth from 0.0083 – 100 Hz (0.01 – 120 s). The tests were performed for a recording time of 1-2 hr with a sampling rate of 200 Hz. The sensors were generally partially buried 51-102 mm, where possible, to improve coupling with the ground, and always covered with a 19-L bucket to reduce external noise such as wind. Figure 3 shows the set-up of two different sensors, one that was mounted on the surface, and the other buried below ground.

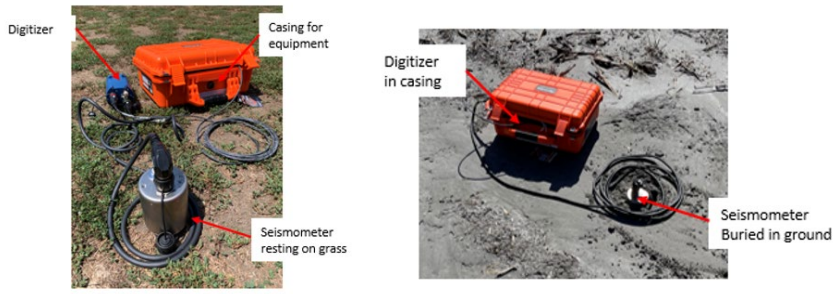

Figure 3. Example field deployment of the sensors used for this study showing surface and partially buried configurations

The data processing procedures used in the calculation of mHVSR ordinates are adapted from Wang et al. (2022b) as described by Ornelas et al. (2024). These procedures are not repeated here for brevity. Figure 4 shows an example smoothed mHVSR mean curve and standard deviation for the Martinez site (i.e., site 2 in Figure 2a). This site has a significant low-frequency peak, at about 0.7 Hz, which will be discussed further below.

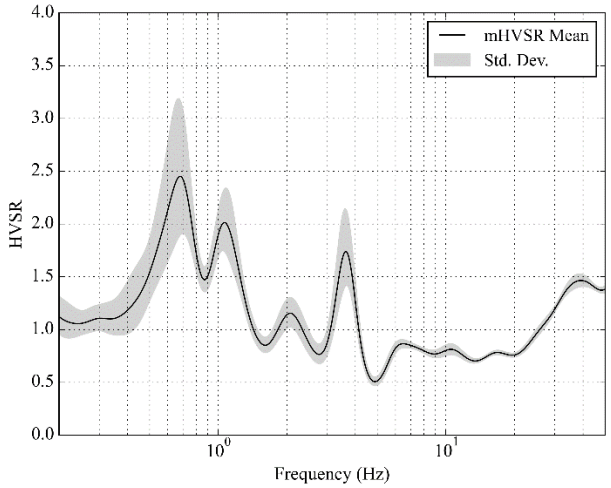

Figure 4. Computed mean mHVSR curve for a station 2.0.0 at site 2 Benicia-Martinez, showing an example of a processed mHVSR curve.

Correlation metric for evaluation of spatial variability in HVSR

Processed mHVSR data for each location in the circular arrays was evaluated for similarity to the center mHVSR curve closest to the vertical array. This evaluation began with visual inspections of the data by three different analysts (the three authors of this paper) to qualitatively assess compatibility of the curves and to determine how their correlation might be measured. We decided to consider mHVSR ordinates within frequency intervals, with each frequency interval represented a bin with a peak in any of the mHVSR curves at the site. The mHVSR curves were also organized by radial distance from the vertical array (50, 100, 250, 500 m).

Analysts visually inspected the mHVSR curves of all sites for each distance and frequency bin and qualitatively evaluated the similarity between the mHVSR closest to the vertical array (i.e.,

the reference 0.0 test) and the mHVSR curves at different radial distances. Figure 5 shows an example of two sites that the analysts inspected (the sites in Figure 2). Figure 5a is an example of mHVSR curves judged to be spatially similar, meaning that the majority of the curves (shown in grey) have similar shapes and amplitudes, compared to the reference mHVSR curve (shown in red) for the first two frequency intervals. Figure 5b is an example of mHVSR curves judged to be spatial variable, due to vertical spacing of their ordinates (in this case the shapes are similar). Other sites judged to be spatially variable had curves with different shapes relative to the reference curve, suggesting more pronounced geologic complexity.

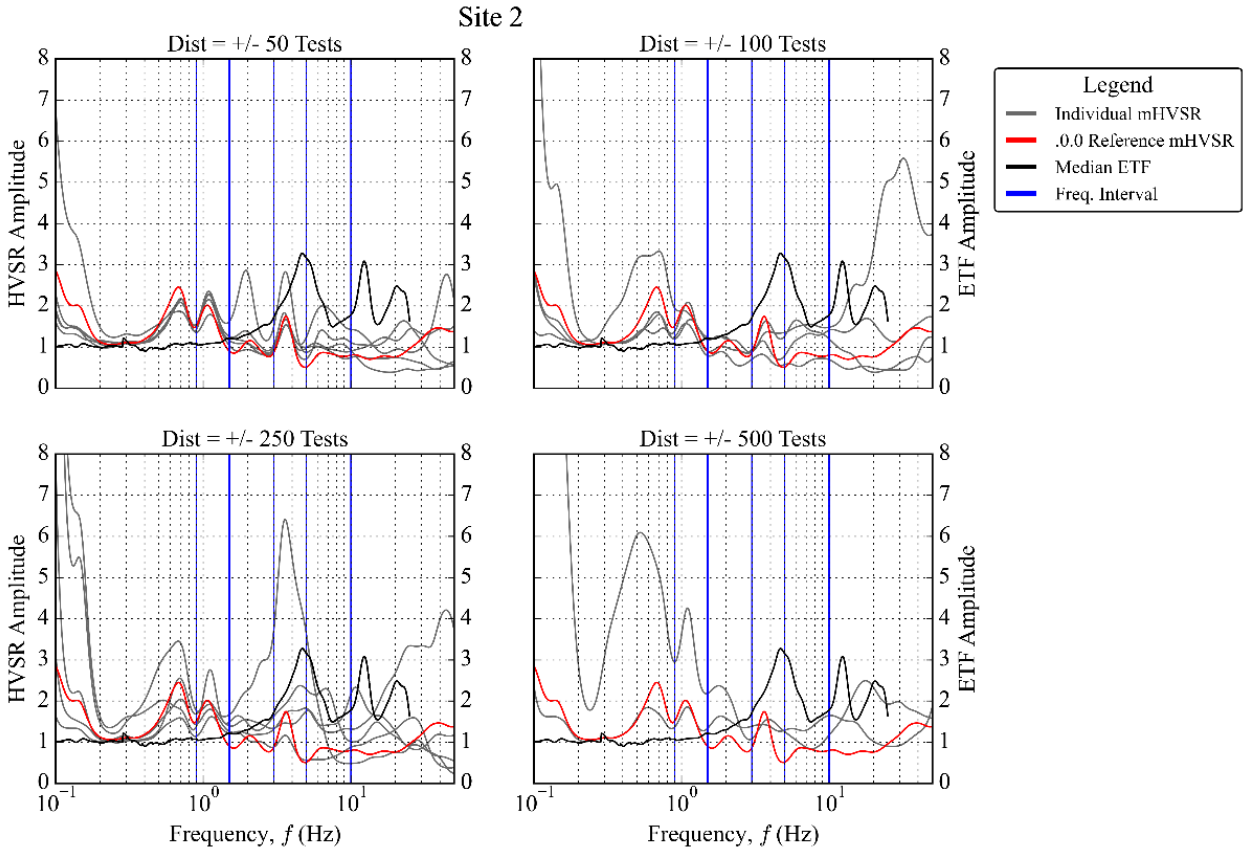

Figure 5a. Mean mHVSR curves from Benicia-Martinez (site 2) for the central station (red line) and four radial distances (gray lines). The black curve denotes the ETF from the vertical array. The blue lines indicate different frequency intervals associated with distinct resonant peaks.

Because the analysis of spatial variability of mHVSR is used subsequently to investigate the effectiveness of 1D GRA, we felt it was useful for the plots in Figure 5 to depict the empirical transfer functions (ETFs) derived from vertical arrays, which demonstrate the frequency range over which site response was measured. The ETFs were computed as described in the following section and are shown in black in Figure 5. Our rationale is that the spatial correlations of mHVSR ordinates are presumably most relevant for investigations of GRA over the frequency range (e.g., fundamental mode frequency) as revealed by ETF ordinates. However, we did not consider ETF

attributes when selecting the frequency intervals used to assess correlations between different mHVSR curves.

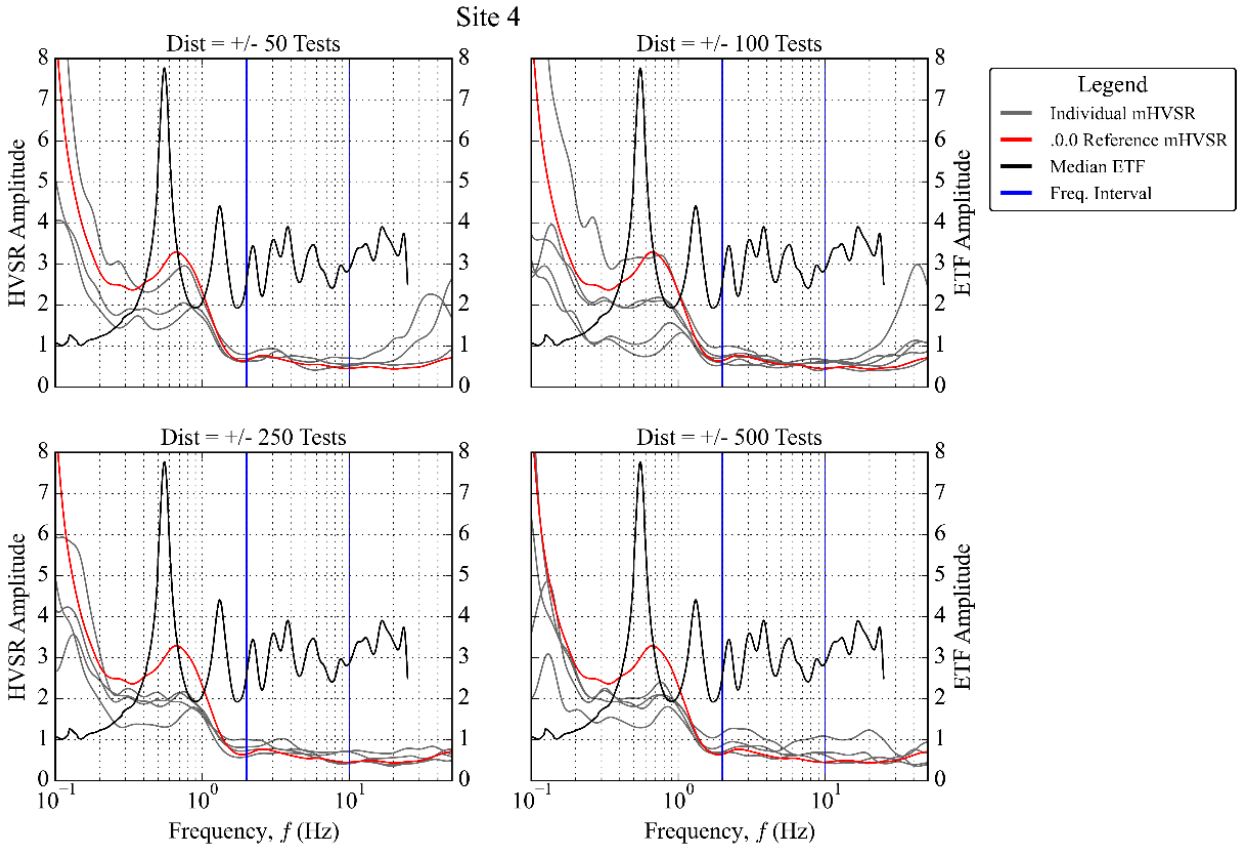

Figure 5b. Mean mHVSR curves from El Centro-Meloland (site 4) for the central station (red line) and four radial distances (gray lines). The black curve denotes the ETF from the vertical array. The blue lines indicate different frequency intervals associated with distinct resonant peaks.

For each of the considered frequency intervals, analysts assigned values of 0 to 3 based on their assessment of the similarity of mHVSR curves at a given radial distance from the center station. The indices indicate the following:

0. No peak was present in the reference curve in the frequency range
1. The curves were poorly correlated
2. Intermediate levels of correlation between curves for the frequency range and radial distance
3. The curves were well correlated for the frequency range and radial distance

Because the indices are qualitative and user-dependent, we sought to identify correlation metrics that could be computed directly from the data and provide similar results for the various radial distances and frequency bins. Four correlation metrics were considered, three of which appeared to best match the analysts' visual assessments. These three metrics are:

- Longest Common Subsequence, LCSS (e.g., Vlachos et al. 2002)

- Pearson's sample correlation coefficient *r* (e.g., Benesty et al. 2009)
- Mean Absolute Error (e.g., Willmott et al. 2005)

The association of the analyst-defined indices with correlation metrics is represented in Figure 6, in which histograms are presenting showing the binned occurrences of the selected metrics for results having a given index (0, 1, 2, 3). In Figure 8, strong agreement between the analysts' indices and the metrics is provided by high values of LCSS correlation and Pearson's correlation, and low values of maximum absolute error (MAE), for index 3 data and the opposite trends for index 1 data. All three correlation metrics demonstrate such trends, but to varying degrees. Ultimately, we selected the LCSS correlation due to the visually strongest trends with analysts' indices.

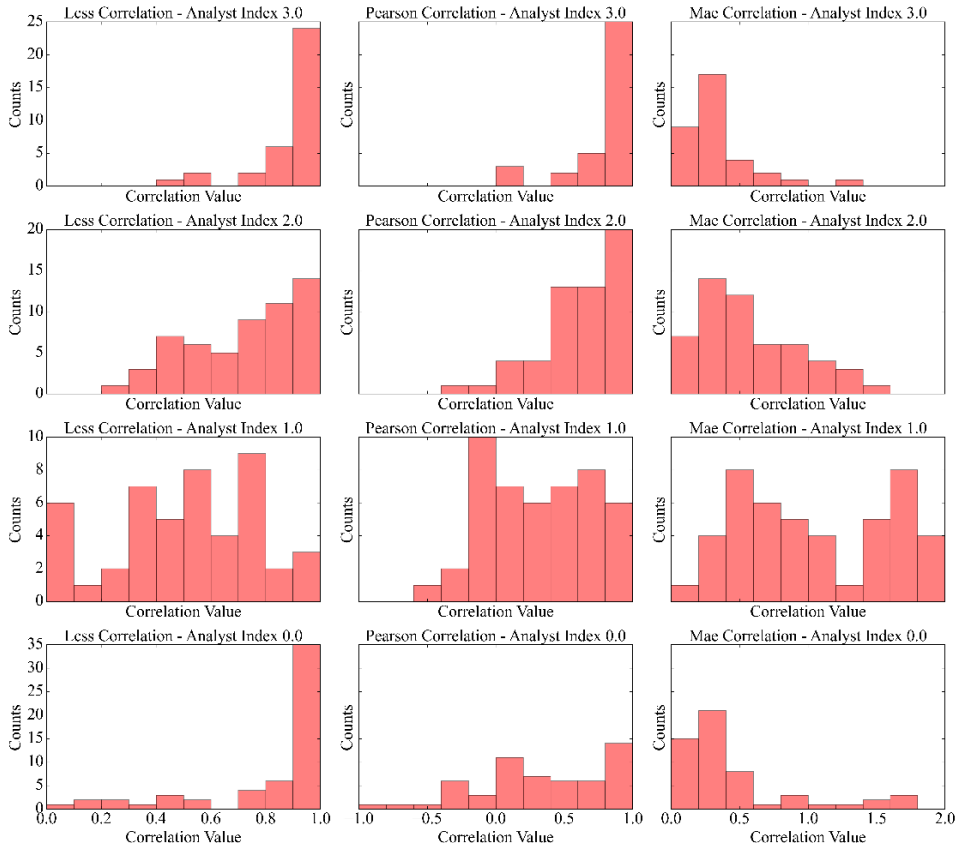

Figure 6. Histogram showing the distribution of values for three different correlation models: Pearson r coefficient, Mean Absolute Error (MAE), and Longest Common SubSequence (LCSS). These histograms compare the choices by analyst with what the values calculated by the correlation models.

The LCSS metric, typically denoted *S* as shorthand for "similarity value," is computed as follows (Vlachos et al. 2002):

$$S(A, B, \epsilon, \delta) = \frac{LCSS_{\delta,\epsilon}(A,B)}{min(n,m)} \quad (1)$$

where A and B are arrays of mHVSR ordinates of size $n \times 2$ and $m \times 2$, respectively (n and m indicate the number of frequencies in each array and 2 reflects that the arrays have one column for frequencies and one for amplitudes), ϵ is a user-selected matching threshold that ranges from 0 to 1, δ is a radius parameter that controls (for a given point with a given reference frequency) the frequency range around the reference where a match can be sought, and the $LCSS_{\delta,\epsilon}$ operator evaluates the match between paired points between the arrays. We utilize the python library *tslearn* (Tavenard et al. 2020) to compute S between the two mHVSR curves across selected frequency intervals.

Figure 7 shows two HVSR curves (labeled as "ref" and "meas") and lines between them to illustrate how the $LCSS_{\delta,\epsilon}$ operator functions. In both cases, matches between paired points are evaluated. The pairing can occur vertically, as in the case of the green lines indicated in Figure 7 as $\epsilon = 1$, or it can occur across frequencies as indicated by the blue lines ($\epsilon = 0.5$). For a given threshold, the algorithm looks for the optimal pairing to evaluate similarity. If the curves are close together (overlayed) then all the points are perfectly paired; for this condition, $LCSS_{\epsilon,\delta}$ will return an integer representing the number of points that were matched between the two curves, causing S to be unity per Eq. (1). As the number of paired points decreases, $LCSS_{\delta,\epsilon}$ decreases, causing S to drop below unity. The degree to which pairings can consider points across frequencies is controlled jointly by the ϵ and δ parameters, with pairings across frequencies increasing as ϵ and δ decrease. We considered this feature of the $LCSS_{\delta,\epsilon}$ metrics to be advantageous relative to the other metrics, as one can select ϵ and δ for use with the algorithm in order to align the algorithms outcomes to users preferences from visual assessment of the data. The δ parameter is referred to in literature as the Sakoe-Chiba (Sakoe and Chiba 1978) radius (also called the warping window size). This radius influences how far in frequency space point pairings can occur between curves, taking into account slight differences in the curves caused by external factors (e.g., noise in time series data). Algorithm run time increases as δ increases because more frequencies need to be interrogated for potential matches. For the present study we used a $\delta = 10$; as shown in Figure 7 for this value of δ, matches across frequencies are made for $\epsilon < 1$ but not for $\epsilon = 1$.

The matching threshold parameter ϵ and range parameter δ affect the $LCSS_{\delta,\epsilon}(A, B)$ calculation as follows:

$$LCSS_{\delta,\epsilon}(A, B, \epsilon, \delta) =$$

$$\begin{cases} 0 & A \text{ or } B \text{ empty} \\ 1 + LCSS_{\delta,\epsilon}(A_{1:n-1}, B_{1:m-1}) & |A_{1,i} - B_{1,j}| < \epsilon \;\&\; |A_{2,i} - B_{2,j}| < \epsilon \;\&\; |i - j| \leq \delta \\ max\left(LCSS_{\delta,\epsilon}(A_{1:n-1}, B), LCSS_{\delta,\epsilon}(A, B_{1:m-1})\right) & otherwise \end{cases} \quad (2)$$

In Eq. (2), $A_{1:n-1}$ is the array A but with its last row removed (hence its length is n-1), which is referred to by Vlachos et al. (2002) as the *head*(A). $B_{1:m-1}$ is similarly defined as array length m-1. $A_{1,i}$ and $A_{2,i}$ refer to the frequency and amplitude in array A for row i, which is an index between 1 and the array length ($B_{1,j}$ and $B_{2,j}$ are similarly defined using index j). The second line on the right side of Eq. 2 seeks matches by taking the absolute differences (in both frequency and amplitude) between points in arrays A and B; if those differences are $< \epsilon$, then the $LCSS_{\delta,\epsilon}$ count increases by 1. If the absolute differences are $> \epsilon$, then the maximum is used (third line on the right

side of Eq. 2). The default value of ϵ is 1, which matches points at the same frequencies, as shown in Figure 7. Vlachos et al (2002) indicated that the determination of ϵ is application dependent, and a value of 1 indicates the curves are relatively similar. Selecting ϵ lower than 1, would allow the algorithm to search further along the curve to make a match, as shown in Figure 7. For the present study we used $\epsilon = 0.75$.

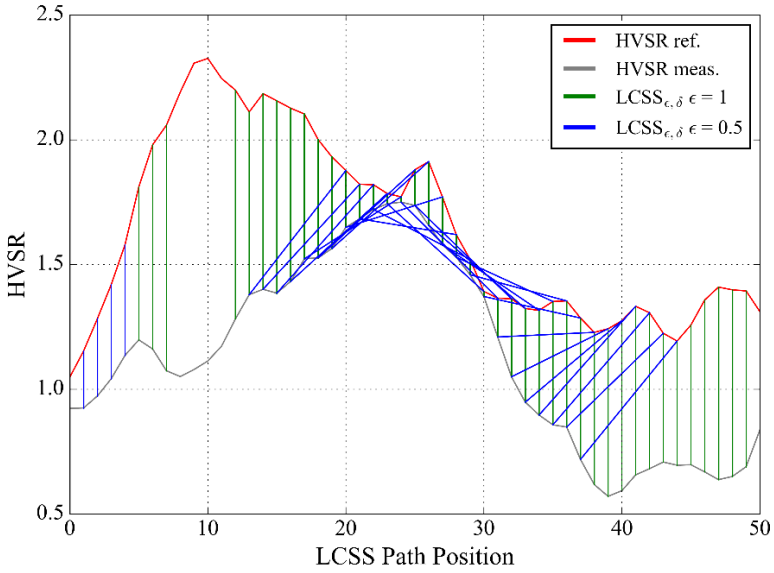

Figure 7. Comparison of two mean HVSR curves, showing the differences in LCSS paths for two different matching thresholds. LCSS path position (x-axis) indicates the index value for which HVSR amplitude is sampled, and corresponds to a specific frequency. The LCSS paths identify the points used to derive similarity between curves.

Interpretation of Vertical Array Seismic Data

As noted in the *Introduction*, previous studies have evaluated the effectiveness of 1D GRA using data from vertical array sites in Japan and California. Many of these validation studies have found that the site response predicted by 1D GRA does not accurately capture observed transfer functions from appreciable fractions of the vertical array sites. Several of the validation studies investigated whether direct modeling of multidimensional effects such as wave scattering (Thompson et al. 2012; de la Torre et al, 2022), non-vertical incidence (Thompson et al. 2012), and laterally-varying soil/rock layers (Hallal and Cox 2020) improve site response predictions at vertical array sites, with mixed results. For the purposes of the present study, we retain the use of 1D GRA as the basis of comparison to empirical transfer functions.

Due to the potential for improved insights from the $LCSS_{\delta,\epsilon}$ metric (Eq. 1), we have re-assessed the compatibility of empirical transfer functions (ETF) from vertical array data and theoretical transfer functions (TTF) from 1D GRA. Both ETFs and TTFs considered here are taken

from de la Torre et al. (2022) for the California vertical array sites considered in Afshari and Stewart (2019).

In de la Torre et al. (2022), ETFs were computed as the ratio of the Fourier amplitude spectrum (FAS) for the observed ground surface motion to the FAS for the downhole motion for each event. For each frequency, the median and lognormal standard deviation were calculated across the data for all events. These ETFs can be considered as the ratio of an outcropping motion (from the surface) to a within motion (at depth). TTFs were computed using 1D GRA in Opensees (McKenna 2011) with viscoelastic material properties to model the linear site response, consistent with the weak ground motions considered for the ETF. TTFs can be derived using either within or outcropping representations of the input motion. Both the median ETF and TTF were smoothed using Konno and Ohmachi smoothing (Konno and Ohmachi 1998) with a smoothing bandwidth of 100.

We applied the procedure described in the previous section for evaluating correlations between mHVSR curves to examine correlations between TTFs and ETFs. This was done for different frequency intervals corresponding to modal frequencies in the TTF and ETF. Results for all sites are summarized in Table 2 and example results for the same two sites considered previously are shown in Figure 8. The mean mHVSR curves for the reference tests are also presented in the figures, which will be discussed subsequently. TTFs based both on within- and outcropping input motions are shown in Figure 8, although the fit assessments used only the within TTF results, which are the theoretically correct choice for application of 1D GRA (Kwok et al. 2007).

For site 2 (Benicia-Martinez South), as shown in Figure 8a, the ETF and TTF peaks align. This suggests good correlation, which is confirmed by an LCSS S value of 0.76 (Table 2). The alignment of peaks is less favorable for site 4 (El Centro-Meloland), which has $S = 0.36$. Results for all sites are provided in Table 2. We interpret $S > 0.6$ as a good fit, which occurs for 53% of sites. We interpret $S < 0.45$ as poor fit, which occurs for 35% of sites. Values of S between 0.45 and 0.6 are considered to have an intermediate ETF-TTF correlation, which occurs for 12% of sites.

The variability column in Table 2 is based on the between-event standard deviation of ETFs over the first frequency interval (denoted $\sigma^{M}_{\ln ETF}$). For reference, we note that previous studies (Thompson et al. 2012; Tao and Rathje 2020a) have used $\sigma^{M}_{\ln ETF} = 0.35$ as a threshold value distinguishing low and high variability, although for a different level of smoothing than that used here. Based on that threshold, 42% of sites have high variability. Two sites experienced low variability, but poor fit, and four sites experienced high variability, but a good fit.

Table 2. Correlations of ETF and TTF and mHVSR based on LCSS metric as evaluated in this study using first-model frequency interval. For mHVSR, the *S* values are averaged over all considered distance intervals.

Station No.	Station Name	HVSR S Value[1]	ETF-TTF S Value[1]	$\sigma^{M}_{\ln(ETF)}$ [1]	Goodness-of-fit
2	Benicia-Martinez South	0.860	0.759	0.325	Good
3	Crockett-Carquinez	0.666	0.639	0.420	Good
4	El Centro-Meloland	0.679	0.358	0.282	Poor
7	Hollister	0.454	0.342	0.461	Poor
8	Hayward-San Mateo	0.953	0.670	0.343	Good
9	La Cienega	0.967	0.771	0.318	Good
10	Obregon Park	0.998	0.517	0.373	Intermediate
11	San Bernardino	0.961	0.722	0.379	Good
12	Vallejo-Hwy 37	0.940	0.441	0.468	Poor
13	Wildlife Liquefaction Array	0.979	0.726	0.228	Good
14	Antioch-San Joaquin S.	0.762	0.730	0.291	Good
15	Corona	0.500	0.421	0.341	Poor
16	Coronado East	0.989	0.720	0.362	Good
17	Coronado West	0.975	0.686	0.362	Good
18	Foster City-San Mateo	0.686	0.505	0.259	Intermediate
19	Hayward-580W	0.576	0.333	0.340	Poor
20	San Francsico Bay Bridge	0.370	0.448	0.308	Poor

1. Derived using first-mode frequency interval

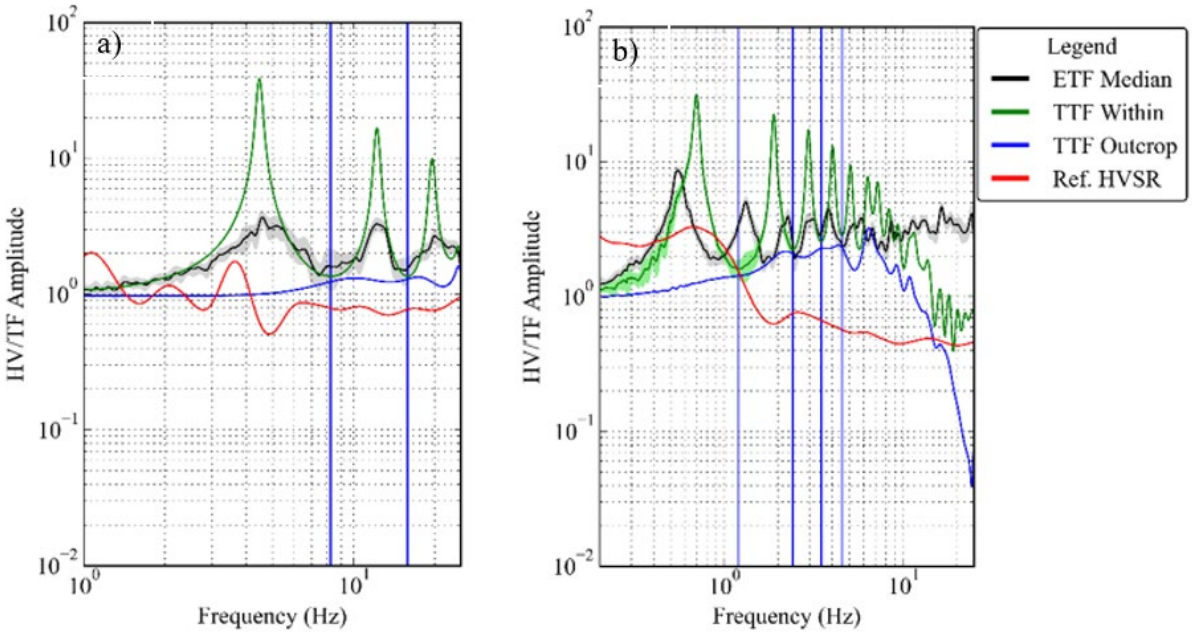

Figure 8. Comparison of empirical transfer function (ETF) with theoretical transfer functions derived using within and outcropping representations of input motions: (a) site 2 results showing generally good correlation and (b) site 4 results showing poor correlations.

Relationship between GRA Effectiveness and mHVSR Correlation

The mHVSR correlation metrics can be examined from a number of perspectives to evaluate their consistency with respect to frequency and separation distance. However, for this paper, we focus solely on their relationship to GRA effectiveness, as represented in the prior section.

Figure 9 compares *S* values derived for the first-mode frequency interval from the ETF-TTF and the closest associated frequency interval in mHVSR, using values from Table 2. The positive correlation between the *S* values supports the hypothesis that mHVSR spatial correlation is predictive of 1D GRA effectiveness, as represented by ETF-TTF *S* values. In particular, mHVSR *S* values > 0.8 correspond to *S* > 0.6 for ETF-TTF (indicating favorable effectiveness of 1D GRA) in 6 out of 8 cases (75%). At the other end of the scale, mHVSR *S* values < 0.6 correspond to ETF-TTF *S* values < 0.45 in 5 of 5 cases (100%). As a result, we consider the spatial variability of mHVSR measurements to have promise as an indicator for 1D GRA effectiveness. Further research will refine these relationships, including data from additional sites and investigation of their dependence on distance intervals.

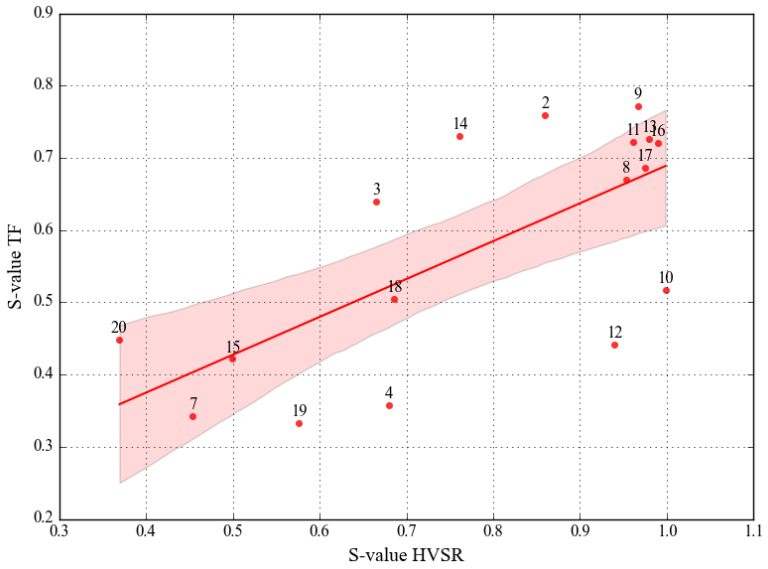

Figure 9. Relationship between *S*-values for first frequency interval in the ETF-TTF data and the closest associated mHVSR frequency interval in mHVSR averaged over the radial distances available from the mHVSR instrument arrays. Shaded region indicates a 95% confidence interval for the trend. These correlations illustrate the predictive capacity of mHVSR spatial correlation on 1D GRA effectiveness.

As part of assessing the relationship between mHVSR and site response as revealed by the vertical arrays, it is useful to examine the relationships between the mean ETF and mean mHVSR curves. Two examples of such comparisons are provided in Figure 8. In the case of site 4, the lowest frequency peaks are close to aligning, whereas for site 2 they do not (the lowest mHVSR peak near 1 Hz is at a lower frequency). If the portion of the profile that controls site response is

included within the depth range of the vertical array, then reasonable alignment of peaks is expected. This appears to be the case with site 4, which has an unusually deep vertical array (~ 195 m), even though the site is in a very deep basin that extends beyond the base depth of the array. It is likely that the resonant frequency associated with the overall basin thickness is lower than the lower-frequency limit of the mHVSR curve, which is not unusual (Ornelas et al. 2024). In the case of site 2, the base of the array is located in blue hard shale, which has a $V_{s,DH}$ = 600 m/s (where DH signifies downhole sensor). Within the domain of the vertical array, the hard shale does not have a significant impedance contrast, which likely occurs at greater depth, which would explain the lower frequency resonances seen in the mHVSR curve for the site.

Conclusions

This study has demonstrated that microtremor horizontal-to-vertical spectral ratio (mHVSR) spatial correlation may serve as an effective indicator for assessing the reliability of 1D GRA. Utilizing a dataset of 300 microtremor recordings from 17 vertical downhole array sites across California, we investigated the spatial variability of mHVSR through three correlation metrics: Longest Common Subsequence (LCSS), Pearson's *r* Coefficient, and Mean Absolute Error (MAE). Among these, we recommend LCSS as the preferred metric to characterize spatial variability, due to its ability to more effectively represent analyst judgment. Our findings revealed that 75% of the sites that exhibited a high degree of spatial correlation from mHVSR using the LCSS metric in Eq. (1) (denoted *S*) had observed site responses from vertical arrays that were well modelled by 1D GRA. Moreover, 100% of sites that exhibited a low degree of spatial correlation in mHVSR were not well modelled by 1D GRA. The analyses concentrated on frequency intervals encompassing low-frequency peaks in both the transfer function and HVSR, with higher frequency peaks showing diminished correlation, likely influenced by interference from cultural noise. This research presents a promising, cost-effective approach for evaluating site spatial variability in the absence of more extensive, and costly invasive site characterization data. Further investigations are needed to refine these relationships using additional data and to explore their dependence on distance and frequency.

Acknowledgements

This study was partially supported by Pacific Gas and Electric (PG&E), and we sincerely appreciate their generous support. Contributions of the second author were supported by the New Zealand National Hazards Commission (previously EQC). We would also like to express our gratitude to the California Strong Motion Instrumentation Program (CSMIP) for their funding of our ongoing work on site response modeling conditioned on HVSR. Finally, we extend our thanks to our HVSR working group for their valuable information exchange and constructive feedback.

References

Afshari, K., Stewart, J. P., & Steidl, J. H. 2019. California ground motion vertical array database. *Earthquake Spectra*, 35, 2003-2015.

Afshari, K., & Stewart, J. P. 2019. Insights from California vertical arrays on the effectiveness of ground response analysis with alternative damping models. *Bulletin of the Seismological Society of America*, 109(4), 1250–1264.

Bahrampouri, M., & Rodriguez-Marek, A. 2023. One-dimensional site response analysis: Model error estimation. *Bulletin of the Seismological Society of America*, 113(1), 401–416. https://doi.org/10.1785/0120210291

Benesty, J., Chen, J., Huang, Y., & Cohen, I. 2009. Pearson correlation coefficient. In *Noise reduction in speech processing* (pp. 37–40). Springer.

Buckreis, T. E., Stewart, J. P., Brandenberg, S. J., & Wang, P. 2024. Small-strain site response of soft soils in the Sacramento-San Joaquin Delta region of California conditioned on V_{S30} and mHVSR. *Earthquake Spectra*. https://doi.org/10.1177/87552930231217165

Ghofrani, H., Atkinson, G. M., & Goda, K. 2013. Implications of the 2011 M9.0 Tohoku Japan earthquake for the treatment of site effects in large earthquakes. *Bulletin of Earthquake Engineering*, 11, 171–203.

Hallal, M. M., & Cox, B. R. 2020. An H/V geostatistical approach for building pseudo-3D Vs models to account for spatial variability in ground response analyses I: Model development. *engrXiv*. https://doi.org/10.31224/osf.io/42yw9

Kaklamanos, J., Bradley, B.A., Thompson, E.M., Baise, L.G. 2013. Critical parameters affecting bias and variability in site-response analyses using KiK-net downhole array data, *Bulletin of the Seismological Society of America*, 103, 1733–1749.

Konno, K., & Ohmachi, T. 1998. Ground-motion characteristics estimated from spectral ratio between horizontal and vertical components of microtremor. *Bulletin of the Seismological Society of America*, 88, 228–241.

Kwak, D. Y., Ahdi, S. K., Wang, P., Zimmaro, P., Brandenberg, S. J., & Stewart, J. P. 2021. Web portal for shear wave velocity and HVSR databases in support of site response research and applications. *UCLA Geotechnical Engineering Group*. https://doi.org/10.21222/C27H0V

Kwok, A. O., Stewart, J. P., Hashash, Y. M. A., Matasovic, N., Pyke, R., Wang, Z., & Yang, Z. 2007. Use of exact solutions of wave propagation problems to guide implementation of nonlinear seismic ground response analysis procedures. *Journal of Geotechnical and Geoenvironmental Engineering*, 133(11), 1385-1398.

Lachet, D., Hatzfeld, C., Bard, P.-Y., Theodulis, N., Papaioannou, C., & Savvaidis, A. 1996. Site effects and microzonation in the city of Thessaloniki (Greece): Comparison of different approaches. *Bulletin of the Seismological Society of America*, 86, 1692–1703.

Lermo, J., & Chávez-García, F. J. 1993. Site effect evaluation using spectral ratios with only one station. *Bulletin of the Seismological Society of America*, 83, 1574–1594.

McKenna, F. 2011. OpenSees: A framework for earthquake engineering simulation. *Computing in Science & Engineering*, 13(4), 58–66.

Molnar, S., Cassidy, J. F., Castellaro, S., et al. 2018. Application of microtremor horizontal-to-vertical spectral ratio (MHVSR) analysis for site characterization: State of the art. *Surveys in Geophysics*, 39(4), 613–631.

Nakamura, Y. 1989. A method for dynamic characteristics estimation of subsurface using microtremors on the ground surface. *Quarterly Report of Railway Technical Research Institute*, 30, 25-33.

Nogoshi, M., & Igarashi, T. 1971. On the amplitude characteristics of microtremor (part 2). *Journal of Seismological Society of Japan*, 24, 26–40 (In Japanese with English abstract).

Ornelas, F. G., de la Torre, C., Nweke, C., Buckreis, T., Wang, P., Bradley, B., Brandenberg, S. J., & Stewart, J. 2023. Microtremor horizontal-to-vertical spectral ratio (mHVSR) data collection at California downhole vertical array sites, 2022. In *Microtremor Horizontal-to-Vertical Spectral Ratio (mHVSR) Site Characterization of California Vertical Arrays*. *DesignSafe-CI*. https://doi.org/10.17603/ds2-by4m-ed67.

Ornelas, F. G., Nweke, C. C., de la Torre, C. A., Wang, P., Mai, T. D., Cox, B. R., Brandenberg, S. J., & Stewart, J. P. 2024. Reliability of low frequency mHVSR ordinates. *18th World Conference on Earthquake Engineering Conference*, Italy.

Pilz, M., & Cotton, F. 2019. Does the one-dimensional assumption hold for site response analysis? A study of seismic site responses and implications for ground motion assessment using KiK-Net strong-motion data. *Earthquake Spectra*, 35(2), 883–905.

Pinilla-Ramos, C., Abrahamson, N., & Kayen, R. 2022. Estimation of site terms in ground-motion models for California using horizontal-to-vertical spectral ratios from microtremor. *Bulletin of the Seismological Society of America,* 112(6), 3016–3036.

Sakoe, H., & Chiba, S. 1978. Dynamic programming algorithm optimization for spoken word recognition. *IEEE Transactions on Acoustics, Speech, and Signal Processing*, 26, 43-49. https://doi.org/10.1109/TASSP.1978.1163055

Site Effects Assessment using Ambient Excitations (SESAME). 2004. Guidelines for the implementation of the H/V spectral ratio technique on ambient vibrations—Measurements, processing and interpretation. *European Commission Project* No. EVG1-CT- 2000-00026, 62. Available at http://sesame.geopsy.org/Papers/HV_User_Guidelines.pdf (last accessed September 2012).

Stewart, J. P., & Afshari, K. 2021. Epistemic uncertainty in site response as derived from one-dimensional ground response analyses. *Journal of Geotechnical and Geoenvironmental Engineering*, 147(1), 04020146.

Tavenard, R., Faouzi, J., Vandewiele, G., Divo, F., Androz, G., Holtz, C., Payne, M., Yurchak, R., Rußwurm, M., Kolar, K., & Woods, E. 2020. Tslearn, a machine learning toolkit for time series data. *Journal of Machine Learning Research*, 21(118), 1-6. http://jmlr.org/papers/v21/20-091.html

Tao, Y., & Rathje, E. M. 2020. Taxonomy for evaluating the site-specific applicability of one-dimensional ground response analysis. *Soil Dynamics and Earthquake Engineering*, 128, 105865.

Teague, D. P., Cox, B. R., & Rathje, E. M. 2018. Measured vs. predicted site response at the Garner Valley Downhole Array considering shear wave velocity uncertainty from borehole and surface wave methods. *Soil Dynamics and Earthquake Engineering*, 113, 339-355. https://doi.org/10.1016/j.soildyn.2018.05.031

Theodulidis, N., Archuleta, R. J., Bard, P.-Y., & Bouchon, M. 1996. Horizontal to vertical spectral ratio and geological conditions: The case of Garner Valley downhole array in southern California. *Bulletin of the Seismological Society of America,* 86, 306–319.

Thompson, E. M., Baise, L. G., Tanaka, Y., & Kayen, R. E. 2012. A taxonomy of site response complexity. *Soil Dynamics and Earthquake Engineering*, 41, 32–43.

de la Torre, C., Bradley, B., Stewart, J., & McGann, R. 2022. Can modelling soil heterogeneity in 2D site response analyses improve predictions at vertical array sites? *Earthquake Spectra*, 38 (4).

Vlachos, M., Gunopoulos, D., & Kollios, G. 2002. Discovering similar multidimensional trajectories. In *Proceedings of the 18th International Conference on Data Engineering* (ICDE '02). IEEE

Wang, P., Tsai, Y. T., Stewart, J. P., Mikami, A., & Brandenberg, S. J. 2022a. Region-specific linear site amplification model for peaty organic soil sites in Hokkaido, Japan. *Earthquake Spectra, 38*(3), 2207-2234.

Wang, P., Zimmaro, P., Buckreis, T. E., Gospe, T., Brandenberg, S. J., Ahdi, S. K., Yong, A., & Stewart, J. P. 2022b. Relational database for horizontal-to-vertical spectral ratios. *Seismological Research Letters, 93*(2A), 1075-1088.

Wathelet, M., Chatelain, J.-L., Cornou, C., Di Giulio, G., Guillier, B., Ohrnberger, M., & Savvaidis, A. 2020. Geopsy: A user-friendly open-source tool set for ambient vibration processing. *Seismological Research Letters, 91,* 1878–1889. https://doi.org/10.1785/0220190360.

Willmott, C. J., & Matsuura, K. 2005. Advantages of the mean absolute error (MAE) over the root mean square error (RMSE) in assessing average model performance. *Climate Research, 30,* 79–82. https://doi.org/10.3354/cr030079.